

Atomistic mechanism of proton conduction in solid CsHSO₄ by a first-principles studyXuezhi Ke^{1,*} and Isao Tanaka^{2,†}¹*Fukui Institute for Fundamental Chemistry, Kyoto University, Kyoto 606-8103, Japan*²*Department of Materials Science and Engineering, Kyoto University, Sakyo, Kyoto 606-8501, Japan*

(Received 20 November 2003; published 15 April 2004)

The electronic structure and proton conduction mechanism of CsHSO₄ in phases I and II have been studied by density-functional theory. The calculated results show that both phases have similar property in the electronic structure. Proton transfer paths and barriers have been investigated by the nudged elastic band method. The similarities and differences of proton transfers in two phases have been discussed. For phase I, the calculated results indicate that the reorientations of the sulfate tetrahedrons can take place frequently, which is in accordance with the experimental observation. For phase II, the highly ordered hydrogen-bond network makes the reorientation of the tetrahedron very difficult. The relatively disordered hydrogen-bond network in phase I plays an important role in the dynamics of tetrahedron, which speeds up proton transfer significantly. The atomistic proton-transfer mechanism in phase I is proposed.

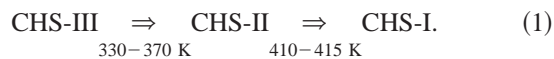
DOI: 10.1103/PhysRevB.69.165114

PACS number(s): 71.15.Mb, 71.20.-b, 66.30.-h

I. INTRODUCTION

During the last few years, proton conductors aroused a great interest because of their applications in energy storage and fuel cell. A key part of fuel cell is the electrolyte, which conducts protons. At low temperature (below 370 K), proton exchange membrane can be applied for the electrolyte.¹ At high temperature (~ 800 – 1200 K), some perovskite-type oxides based on SrCeO₃, BaCeO₃, CaZrO₃, SrZrO₃, and BaZrO₃ exhibit good proton conductivity, and can be used for this purpose.² In the intermediate temperature range of ~ 370 – 800 K, however, there are very few candidates for the solid electrolytes. So there is a gap for this range. Cesium hydrogen sulfate (CHS) such as CsHSO₄ is a potential candidate since it exhibits extremely high proton conductivity above 415 K.³ In 2001 the first fuel cell based on CHS was made and it can operate in the range of ~ 420 – 470 K.⁴

At usual atmospheric condition, CHS has three phases in the temperature range of 123–420 K:^{5–7}



Below 330 K, CHS is in phase III (CHS-III) with a monoclinic structure. At 330–370 K, phase III transforms into phase II (CHS-II) with another monoclinic structure. Above 410 K, phase II transforms into phase I (CHS-I) with a tetragonal structure. Among them, CHS-I shows extremely high proton conductivity (of the order of 10^9 s⁻¹), which is three to four orders of magnitude greater than that in CHS-II.³

Experimentally, proton conductivity in CHS (particularly for CHS-I) has been extensively studied.^{3,8–10} For CHS-I, experimentalists usually consider that proton intrabond jumps and the reorientation of the O-H groups should be responsible for the high conductivity. Theoretically, only a few calculations have been devoted to these materials. So far, no first-principles study has been reported. For CHS-I,

Kreuer *et al.* recently investigated the proton-transfer mechanism in CHS-I using the classical molecular-dynamics simulations.^{11,12} However, as the authors mentioned in their papers that “a physically correct simulation of the hydrogen bond is probably outside the scope of the classical molecular dynamics technique using pair potentials only.” Up to now, some basic questions still are not very clear, e.g., CHS-I and CHS-II have the same chemical formula, why is the proton conductivity in CHS-II significantly lower than that in CHS-I? The atomistic mechanism of proton transfer in these materials has not been well understood either. Such basic information may be useful for the further improvement of proton conductors. Also the investigation of the proton-transfer mechanism in the solid acids is interesting from the academic point of view. Therefore, it is worth studying these materials using the advanced theory.

In this paper, we will focus on CHS-II and CHS-I since CHS-III is only available as a wet material. We have investigated the electronic structure and the proton-transfer mechanism in CHS-I and CHS-II from the first-principles calculations. We found that both phases have similar property in the electronic structure. Proton-transfer paths and barriers are searched without *a priori* knowledge. The similarities and differences of the proton-transfer mechanism between the two phases will be discussed in some detail.

The remainder of this paper is organized in three subsections. In Sec. II, the theoretical method is introduced. In Sec. III, we present the results, in which the electronic structure and the proton diffusion paths and barriers will be discussed. In Sec. IV, the conclusions are summarized.

II. THEORETICAL METHODS

The calculations were performed using the plane-wave basis VASP code,^{16,17} implementing the generalized gradient approximation (GGA) of Perdew and Wang.¹⁸ The interaction between the ion and the electron is described using the projector augmented wave method¹⁹ (PAW) with plane

waves up to a cutoff energy of 400 eV. In the PAW, there is all-electron description of the electronic-ion-core interaction. This method is able to describe bulk properties to the level of accuracy as comparable to FLAPW calculations.²⁰ The configurations $[\text{Kr}]5s^25p^66s^1$ for cesium, $[\text{Ne}]3s^23p^4$ for sulphur, and $[\text{He}]2s^22p^4$ for oxygen were treated as valence electrons, where the core electron configurations are shown in square brackets. Brillouin-zone integrations were performed on the grid of Monkhost-Pack procedure.²¹ For medium size cells ($5.82 \times 5.82 \times 14.64 \text{ \AA}^3$ for CHS-I and $7.94 \times 8.35 \times 7.85 \text{ \AA}^3$ for CHS-II), $3 \times 3 \times 1$ and $2 \times 2 \times 2$ k -point meshes were used for CHS-I and CHS-II, respectively. The convergence for both cases within 10 meV (per unit cell) was achieved (compared with the more dense meshes of $5 \times 5 \times 1$ and $4 \times 4 \times 4$ for CHS-I and CHS-II, respectively). For the larger supercells, only a few k points were used and the convergence within 50 meV was achieved.

To determine proton diffusion barriers and paths, the nudged elastic band method²² (NEB) was used. In the NEB method, a series of the initial images between the two potential minima is chosen, and each image is only allowed to move into the direction perpendicular to the hyp tangent, which is calculated as the normal vector between the two neighboring images. Hence the energy is minimized in all directions except for the direction of the reaction path. A damped molecular dynamics was used to relax ions (until the forces in each image are less than 0.06 eV/\AA) with the time step of 0.01–0.1 fs. After the NEB calculations, a quasi-Newton algorithm was used to refine the obtained results (for the transition states). In the quasi-Newton procedure the forces are minimized rather than the energy. The forces and the stress tensor are used to determine the search directions for finding the equilibrium positions until the forces in all directions of ions are less than 0.04 eV/\AA .

III. RESULTS AND DISCUSSIONS

A. Geometric structures of CHS-I and CHS-II

The computed structure of CHS-II is shown in Fig. 1(b), where the structure parameters are compiled in Table I. It shows that the calculated results agree with the experimental data well within DFT-GGA error. CHS-I belongs to a tetragonal cell with space group $I4_1/amd$. There is no ambiguity about the positions of the heavy cesium ions, but there is debate about hydrogen locations, and consequently the exact orientations of the SO_4 tetrahedrons. Mainly, there are three models proposed by Jirak,²³ Merinov,²⁴ and Belushkin^{25,26} from the experimental observations. In our study,²⁷ we found a model, which is energetically (0.6 eV per cell) more stable than these models. This model is presented in Fig. 1(a) and the lattice parameters are compiled in Table I.

B. Electronic structures of CHS-I and CHS-II

The total and local density of states (DOS) for the perfect CHS were calculated using the tetrahedron method with dense meshes ($8 \times 8 \times 4$ and $8 \times 8 \times 8$ k point for CHS-I and CHS-II, respectively). The results for CHS-I and CHS-II are

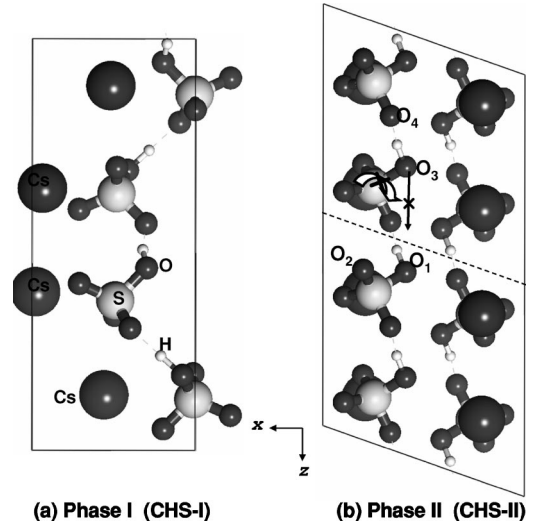


FIG. 1. Crystal structures of CsHSO_4 in phase I (a) and phase II (b). The biggest ball represents cesium ion, the smaller black ball is oxygen, the gray ball is sulphur, and the smallest ball is hydrogen. Note that (b) includes two primitive cells along z direction separated by the dashed line. For CHS-II, the hydrogen-bond network is highly ordered and all the hydrogen bonds are identical crystallographically. In this configuration, it is very difficult to rotate the tetrahedron to form a new hydrogen bond of $\text{O}_1\text{-H}\cdots\text{O}_3$ (a local minimum). Since this rotation will result in the breaking of the hydrogen bond of $\text{O}_3\text{-H}\cdots\text{O}_4$ (see the text for detail).

shown in Figs. 2(A) and 2(B), respectively. Overall, (A) and (B) are quite similar. In the figures, a represents the total DOS and the others are the projected DOS. $\text{O}_1\text{-H}\cdots\text{O}_2$ represents a hydrogen bond, in which H is strongly bound to O_1 and weakly bound to O_2 . O_3 represents an oxygen atom which is not involved in the hydrogen bond. The dashed and dotted lines display the valence-band maximum and the conduction-band minimum, respectively. By the integration projected DOS up to the Fermi level, the total charges of the ions in the hydrogen bond are compiled in Table II.

Since both CHS-I and CHS-II belong to ionic crystals, there should be very limited covalent bonding between Cs and O. However, Figs. 2(A) and 2(B) show that a valence band of Cs $5s$ character is almost the same level as that of O $2s$. This is a mere coincidence and does not mean a strong covalent bonding between Cs and O. This can be verified by visualizing the charge density (not plotted).

For the hydrogen bonding properties, in Fig. 2, d and e clearly show that there is covalent bonding between H and O_1 , and, in Fig. 2, e and f vaguely show that there is little bonding between H $1s$ and O_2 $2s$. This indicates that H is strongly bound to O_1 and only weakly bound to O_2 . There is no bonding between H and O_3 since O_3 is not involved in the hydrogen bond. Quantitatively, Table II shows that the total charge of O_1 is greater than that of O_2 , which in turn is greater than that of O_3 . This is consistent with the hydrogen bonding properties.

The band gaps estimated as the energy difference between the highest occupied and lowest unoccupied one-electron states are 5.26 eV and 5.31 eV for CHS-I and CHS-II, re-

TABLE I. Comparison between the calculated and the experimental structures for CHS-I and CHS-II. The symbol of $O_1-H \cdots O_2$ represents a hydrogen bond, in which H is strongly bound to O_1 and weakly bound to O_2 . For CHS-I, only lattice parameters are listed because for other parameters the different proposal results in the different values.

CsHSO ₄ -II (monoclinic, space group $P2_1/c$)		
Parameter	Calculated	Experiment
a (Å)	7.944	7.781
b (Å)	8.349	8.147
c (Å)	7.851	7.722
β (deg)	109.372°	110.775°
$d(O_1-H)$ (Å)	1.051	0.94(4)
$d(H \cdots O_2)$ (Å)	1.488	1.70(4)
$d(O_1-H \cdots O_2)$ (Å)	2.636	2.526
$\angle O_1HO_2$ (deg)	168.52°	174(6)°
CsHSO ₄ -I (tetragonal, space group $I4_1/amd$)		
Parameter	Calculated	Experiment
a (Å)	5.845	5.741
c (Å)	14.794	14.315
$d(O_1-H)$ (Å)	1.025 or 1.024	
$d(H \cdots O_2)$ (Å)	1.575 or 1.576	
$d(O_1-H \cdots O_2)$ (Å)	2.571 or 2.588	

^aExperiment from Ref. 13.

^bExperiment from Ref. 25.

spectively. Alternatively, it can be calculated as a difference of the total energies of the system with N , $N+1$, and $N-1$ electrons:²⁸

$$E_{gp} = E_{tot}(\text{per})^{+1} + E_{tot}(\text{per})^{-1} - 2E_{tot}(\text{per}), \quad (2)$$

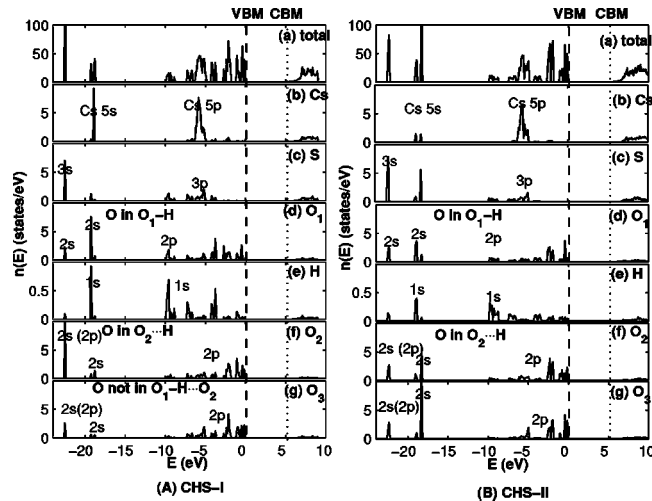


FIG. 2. Density of states (DOS) for CHS-I (A) and CHS-II (B). a is the total DOS and the others including b , c , d , e , f , and g are the projected DOS. $O_1-H \cdots O_2$ represents a hydrogen bond, in which H is strongly bound to O_1 and weakly bound to O_2 . O_3 represents the oxygen ion which is not involved in the hydrogen bond. The dashed and dotted lines display the valence-band maximum (VBM) and the conduction-band minimum (CBM), respectively.

where $E_{tot}(\text{per})$ is the total energy of the perfect neutral supercell, and $E_{tot}(\text{per})^{+1}$ and $E_{tot}(\text{per})^{-1}$ are the total energy of the supercell in the charge states $+1$ and -1 , respectively. The calculated results are compiled in Table III. These values may be more reliable than those from one-electron eigenvalue (note that DFT usually underestimates the band gap²⁹). The band gaps in Table III indicate that both phases are electrical insulators, which is one of the requirements for the fuel cell application.

C. Proton transfer in CHS-I and CHS-II

Proton-transfer paths and barriers were investigated by the NEB method.²² The transfer processes will be discussed by analyzing the transition states and the minimum energy paths. We have systematically investigated the following

TABLE II. Calculated total charges of ions in the hydrogen bond for CHS-I and CHS-II. The symbol of $O_1-H \cdots O_2$ represents a hydrogen bond, in which H is strongly bound to O_1 , and weakly bound to O_2 . O_3 represents the oxygen ion which is not involved in the hydrogen bond. For CHS-I, there are two types of H bonds (just tiny difference). For CHS-II, all the hydrogen bonds are identical.

CHS-I						
$d(O_1-H \cdots O_2)$	$d(O_1-H)$	$d(H \cdots O_2)$	O_2	O_1	O_3	H
2.571	1.025	1.575	5.203	5.180	5.168	0.646
2.588	1.024	1.576	5.198	5.172	5.165	0.653
CHS-II						
2.636	1.051	1.488	5.166	5.141	5.135	0.619

TABLE III. The band gaps for CHS-I and CHS-II estimated from two different methods. One is measured from the energy difference between the highest occupied and lowest unoccupied one-electron states. Another is calculated as a difference of the total energies of the system according to Eq. (2). Note that the first method in DFT usually underestimates the band gap (Ref. 29).

Approaches	CHS-I (eV)	CHS-II (eV)
Measured from one-electron states	5.26	5.31
Calculated from total energies	6.03	6.08

processes: (1) proton transfer within the sulfate tetrahedron, (2) proton transfer within the hydrogen bond, (3) proton transfer to the nearest-neighboring (NN) tetrahedron, and (4) proton transfer to the next-nearest-neighboring (NNN) tetrahedron. The item (4) contains (a) proton rotation and (b) proton diffusion. These almost include all of the possible proton-transfer paths, therefore the obtained results will help us understand the proton-conduction mechanism in these materials. On the basis of these transfer processes, the proton-tunneling effect will be discussed in the end.

1. Proton transfer between the two oxygen ions within the SO_4 tetrahedron

For CHS-I, Fig. 3 presents the successive “snapshots” of proton transfer between the two oxygen ions within the sulfate tetrahedron, and the corresponding energy profile for this process is shown in Fig. 4, in which symbol *a* is the initial state, *b* is the transition state (TS), *c* is the local minimum state, *d* is the TS, *e* is the local minimum, and *f* is the final state. In the TS, proton is located equally between the two oxygen ions, and the distance between the two oxygen

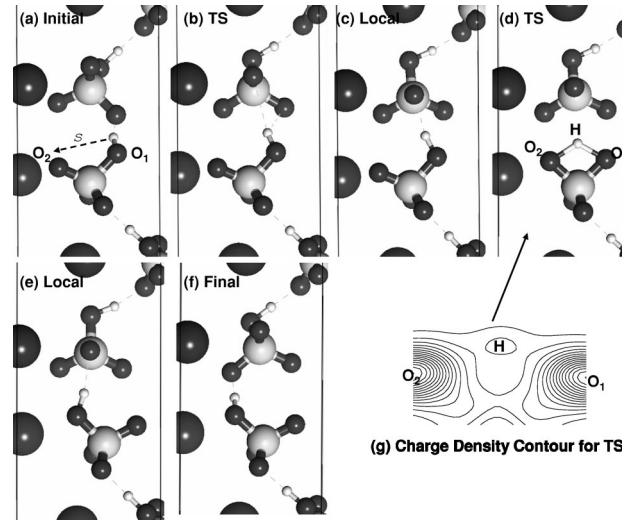


FIG. 3. Successive “snapshots” of proton transfer between the two oxygen ions within the sulfate tetrahedron in CHS-I, in which (a) is initial state, (b) is transition state (TS), (c) is local potential minimum state, (d) is another TS, (e) is another local minimum, and (f) is final state. In the TS (d), proton is located midway between the two oxygen ions. (g) is the electronic charge contour map for the TS (d). The contour plane is defined by one hydrogen and two oxygen ions [denoted as O_1 and O_2 in (d)]. The contour map is enlarged for clarity. The energy profile for this process is shown as a solid line in Fig. 4.

ions [$d(O_1 \cdots O_2) = 2.263 \text{ \AA}$] is shorter than that of the initial state (2.491 \AA). In the other proton-transfer processes, we found that the distance between the two oxygen ions in the TS is always shorter than that of the initial state (actually, it

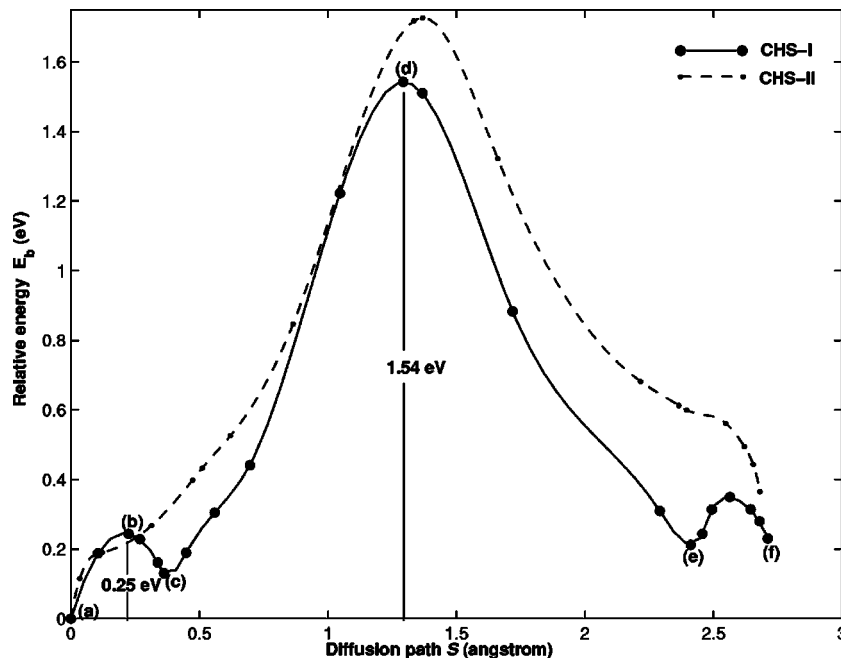


FIG. 4. The energy profile (solid line) for the process in Fig. 3. The diffusion path s is along the arrow in Fig. 3(a). The symbols *a*, *b*, *c*, *d*, *e*, and *f* correspond to the “snapshots” in Fig. 3, in which *a* is initial state, *b* is transition state (TS), *c* is local potential minimum, *d* is another TS, *e* is another local minimum, and *f* is final state. The dashed line represents the similar process in CHS-II.

is the shortest along the diffusion path). This suggests that proton transfer usually is phonon assisted.^{30,31} The interaction in the TS is investigated further by analyzing the charge-density distribution as displayed in Fig. 3(g). The charge contour map shows that proton does not have much interaction with oxygen ions (almost free proton), implying that a large barrier may occur.¹⁴ This is verified in the energy profile. Figure 4 shows that the barrier is as high as 1.54 eV, indicating that this process is almost prohibited (in the temperature range of our interest). Noticeably, there are two local minima including *c* and *e* along the diffusion path. It can be seen from Fig. 4 that proton can reach the local minimum *c* after overcoming a low barrier of 0.25 eV. This means that proton can visit this minimum frequently. In the real diffusion, this indicates that proton does not really diffuse to the other sites, and it just moves forward and then backward with simultaneous reorientations of the sulfate tetrahedron [see Figs. 3(a)–3(c) for the reorientation of the top tetrahedron]. This phenomenon is in accord with the experimental observation by the rf-microwave dielectric measurement, in which the fast reorientations of the sulfate tetrahedrons (10^{12} s^{-1}) were observed.¹⁵

For CHS-II, the energy profile for the similar process is plotted as a dashed line in Fig. 4. It shows that the barrier also is quite high, therefore the process is forbidden too. The curve for CHS-II does not display a local minimum. This is different from that of CHS-I. For CHS-II, Fig. 1(b) shows that the hydrogen-bond network is highly ordered, and all the hydrogen bonds are identical crystallographically. As a result, the formation of a new hydrogen bond of $\text{O}_1\text{-H}\cdots\text{O}_3$ (a local minimum) will cause the breaking of the hydrogen bond of $\text{O}_3\text{-H}\cdots\text{O}_4$ [see Fig. 1(b)]. Thus this makes the rotation of the tetrahedron very difficult. Therefore no local minimum occurs along the diffusion path. Whereas for CHS-I the hydrogen-bond network is disordered to some extent. As a result, a new hydrogen bond can be formed (by rotating one tetrahedron) without breaking other hydrogen bonds [see Fig. 3(c)]. Therefore, the disordered hydrogen-bond network in CHS-I is essential for the dynamics of the tetrahedron in CHS-I.

The essential difference between CHS-I and CHS-II in this process is that proton can reach a local minimum easily in CHS-I, but this is not the case in CHS-II. Due to this local minimum, proton may continue to diffuse to the nearest-neighbor tetrahedron in CHS-I (it will be discussed in the later section). In addition, this local minimum causes the reorientations of the tetrahedrons, it may make the distance between the two oxygen ions in two neighboring tetrahedrons shorter to assist proton transfers.

2. Proton transfer within the hydrogen bond

The simplest proton jump between the sulfate tetrahedrons one may presume is that along the hydrogen bond as shown in Fig. 5. As will be revealed in this section, the energy barrier for this jump is quite low. However, the transfer is confined within the hydrogen bond. In other words, proton can just jump forward and then backward within the hydrogen bond, but it cannot move out of the hydrogen

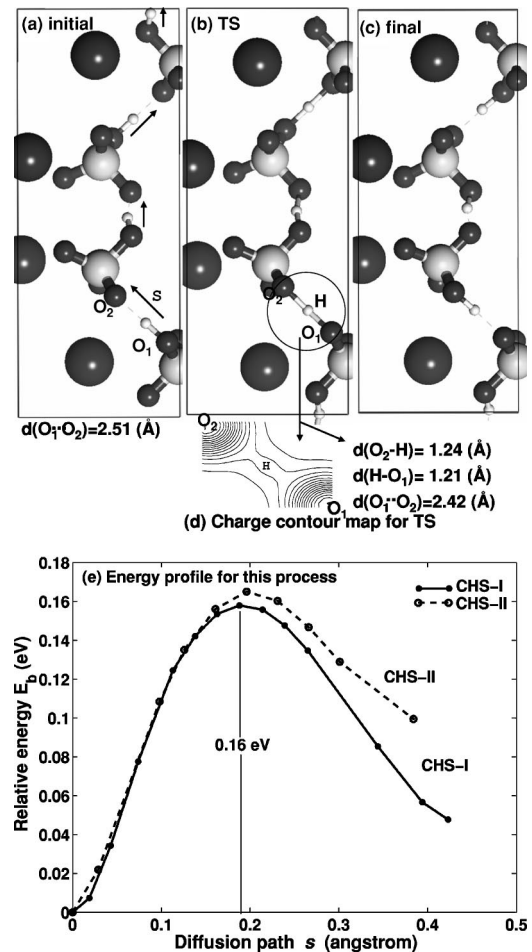


FIG. 5. “Snapshots” of proton transfer between the two oxygen ions within the hydrogen bond in CHS-I. (a), (b), and (c) represent the initial state, the TS, and the final-state configurations, respectively. (d) is the electronic charge density for the TS. The contour map plane is defined by one hydrogen and two oxygen ions. (e) is the corresponding energy profile for this process (solid line). The reaction path s is defined along the arrow in (a). The solid and dashed lines in (e) represent the similar process for CHS-I and CHS-II, respectively.

bond. Therefore the jump cannot contribute to the diffusivity directly. It may facilitate other proton-transfer processes.

First we have investigated a single proton transfer. Only one among four protons per unit cell is made to jump. We found that the energy simply increases along the diffusion path, and there is no local minimum. The energy increase may be ascribed to the formation of H_2SO_4 and SO_4 tetrahedrons out of two HSO_4 . Instead of this, we investigated the concerted transfer, in which several protons diffuse simultaneously as shown in Fig. 5. In our study, we assume that four protons transfer to the next oxygen ions simultaneously under the periodical boundary condition.

For CHS-I, Fig. 5 presents the snapshots of proton transfers between the two oxygen ions within the hydrogen bonds, and the corresponding energy profile for this process is shown as a solid line in (e), in which (a), (b), and (c) represent the initial-state, TS, and final-state configurations, respectively. In the TS, proton is located approximately mid-

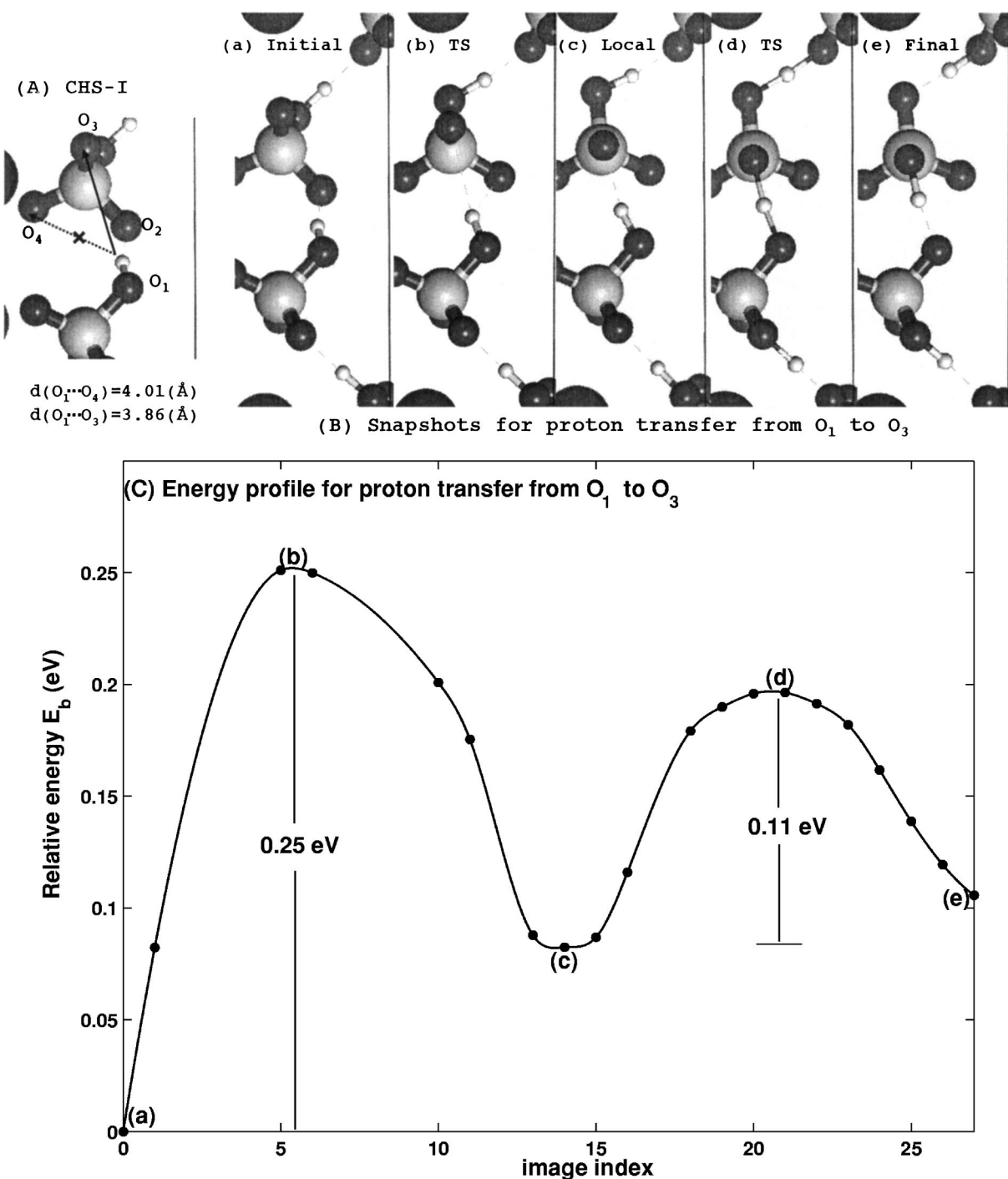


FIG. 6. Proton transfer to the next oxygen ion of the nearest-neighbor (NN) tetrahedron in CHS-I. (A) shows that there are three proton-transfer paths including $O_1 \rightarrow O_2$, $O_1 \rightarrow O_3$, and $O_1 \rightarrow O_4$. The first path ($O_1 \rightarrow O_2$) was feasible. The second path ($O_1 \rightarrow O_3$) also is feasible. The process for $O_1 \rightarrow O_3$ is illustrated as the “snapshots” in (B), and the corresponding energy profile is shown in (C), in which a is initial state, b is TS, c is local potential minimum, d is TS, and e is final state. The reaction path is simply expressed as the image index since it is hard to be coordinated in this case. The third path ($O_1 \rightarrow O_3$) is forbidden (see the text for detail).

way between the two oxygen ions, and the distance between the two oxygen ions [$d(O_1 \cdots O_2) = 2.42 \text{ \AA}$] is shorter than that of the initial state (2.51 \AA). The interaction in the TS is investigated further by analyzing the charge-density distribution as displayed in Fig. 5(d). The charge contour map shows that proton is surrounded by the charges from the two oxygen ions. This means proton has relatively strong covalent

interaction with the oxygen ions, indicating that the barrier may be low. This is verified in the energy profile. Figure 5(e) shows that the barrier is only 0.16 eV.

For CHS-II, the situation is quite similar to that in CHS-I, i.e., a single proton transfer also is forbidden. The concerted transfer is energetically favorable. The energy profile for CHS-II is plotted as a dashed line in Fig. 5(e). The barrier is

0.17 eV.

According to the above investigation, proton transfer within the hydrogen bond is feasible for both phases when the concerted motion is assumed. In the real diffusion, proton transfers will take place along the chemical potential direction (from the high to the low) within the hydrogen bonds.

3. Proton transfer to the next oxygen ion of the nearest-neighboring tetrahedron

For CHS-I, Fig. 6(A) shows that there are three paths for proton transfer to the next oxygen ion of the NN tetrahedron. They include $O_1 \rightarrow O_2$, $O_1 \rightarrow O_3$, and $O_1 \rightarrow O_4$. The first path ($O_1 \rightarrow O_2$) is feasible as discussed in the preceding section of proton transfer within the hydrogen bond. The second path ($O_1 \rightarrow O_3$) also is feasible. The transfer process is illustrated as the snapshots in Fig. 6(B), and the corresponding energy profile is shown in Fig. 6(C), in which symbol *a* is the initial state, *b* is the TS, *c* is the local minimum, *d* is the TS, and *e* is the final state. The process from *a* to *c* is the same as that from Fig. 3(a) to Fig. 3(c). The process from *c* to *e* is similar to that of proton transfer within the hydrogen bond. It can be seen from Fig. 6(C) that from *a* to *c* proton reaches a local minimum after overcoming a low barrier of 0.25 eV, and then from there it continues to transfer to the next oxygen ion with a low barrier of 0.11 eV. As for the third path, $O_1 \rightarrow O_4$, the calculated results show that the minimum energy path follows $O_1 \rightarrow O_2 \rightarrow O_4$. As discussed previously, proton transfer within the sulfate tetrahedron is almost forbidden. Since proton transfer from O_2 to O_4 is within the tetrahedron, therefore this path is virtually forbidden.

For CHS-II, Fig. 7 shows that there also are three paths to the NN tetrahedron including $O_1 \rightarrow O_2$, $O_1 \rightarrow O_3$, and $O_1 \rightarrow O_4$

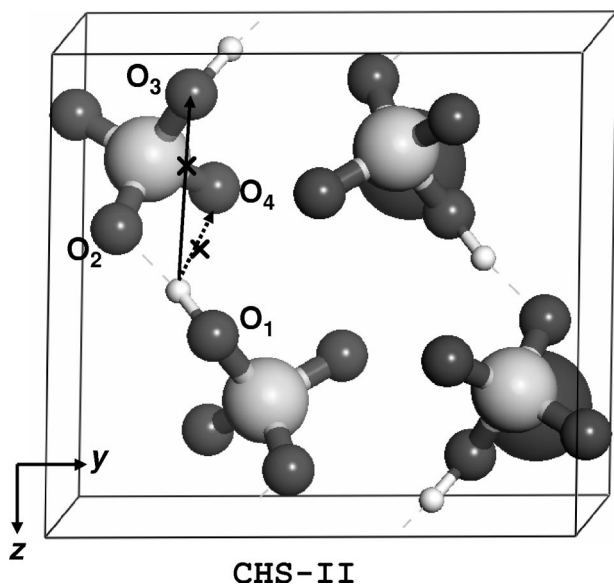


FIG. 7. Proton transfer to the nearest-neighboring tetrahedron in CHS-II. It shows that there are three proton-transfer paths including $O_1 \rightarrow O_2$, $O_1 \rightarrow O_3$, and $O_1 \rightarrow O_4$. The first path ($O_1 \rightarrow O_2$) is feasible as discussed in Sec. III C 2 (proton transfer within the hydrogen bond). The others including $O_1 \rightarrow O_3$ and $O_1 \rightarrow O_4$ are almost forbidden (see the text for detail).

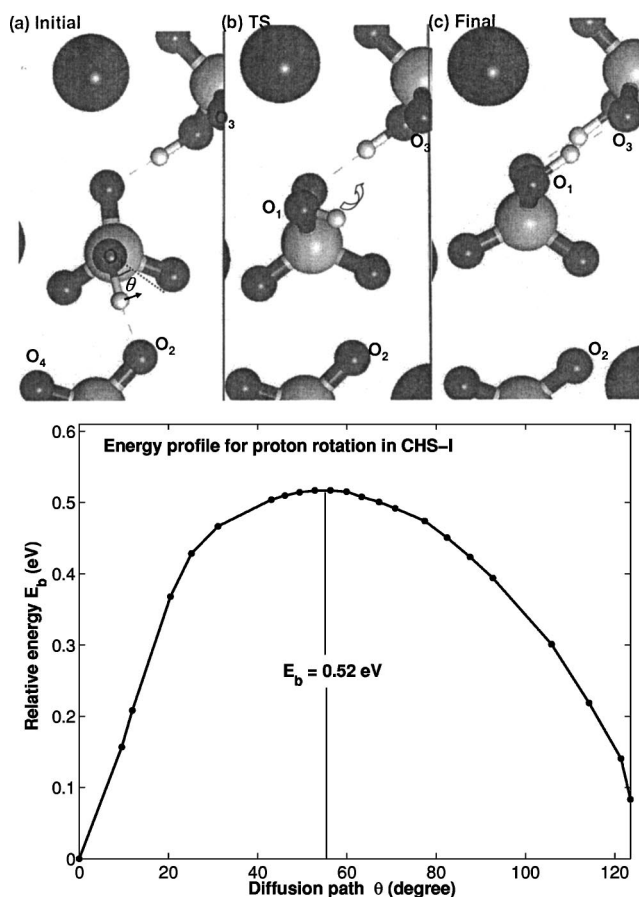


FIG. 8. After proton transfer to the nearest-neighboring tetrahedron in CHS-I (*e* in Fig. 6), it continues to rotate from one hydrogen bond to the next. The process is illustrated as the “snapshots” in (a)–(c). In the initial state (a), proton is located between O_1 and O_2 (forming $O_1\text{-H}\cdots O_2$). In final state (c), proton is located between O_1 and O_3 (forming a new hydrogen bond of $O_1\text{-H}\cdots O_3$). The energy profile for this process is shown in the lower half of the figure. The reaction path θ is defined in the snapshot (a). The barrier for this process is 0.52 eV.

$\rightarrow O_4$. Due to the same reasons as CHS-I, the first path $O_1 \rightarrow O_2$ is feasible and the third path $O_1 \rightarrow O_4$ is forbidden. We found that the second path $O_1 \rightarrow O_3$ also is forbidden. The calculated results show that the minimum energy path follows $O_1 \rightarrow O_2 \rightarrow O_3$. Since proton transfer from O_2 to O_3 is within the tetrahedron, therefore this path is forbidden. This is different from that of CHS-I. The reason is almost the same as before, i.e., the highly ordered hydrogen-bond network in CHS-II makes the formation of a new hydrogen bond of $O_1\text{-H}\cdots O_3$ impossible, thus no local minimum occurs, and consequently the diffusion barrier increases significantly along this path.

According to the above investigation, it shows that only proton in CHS-I can be transferred to the NN tetrahedron. After proton transfers to the NN tetrahedron (*e* in Fig. 6), from there it may continue to rotate from one hydrogen bond to the next. The rotation process is illustrated as the snapshots in Fig. 8, and the energy profile for this process is shown below. In the initial state (a), proton is located between O_1 and O_2 . In the final state (c), proton is located

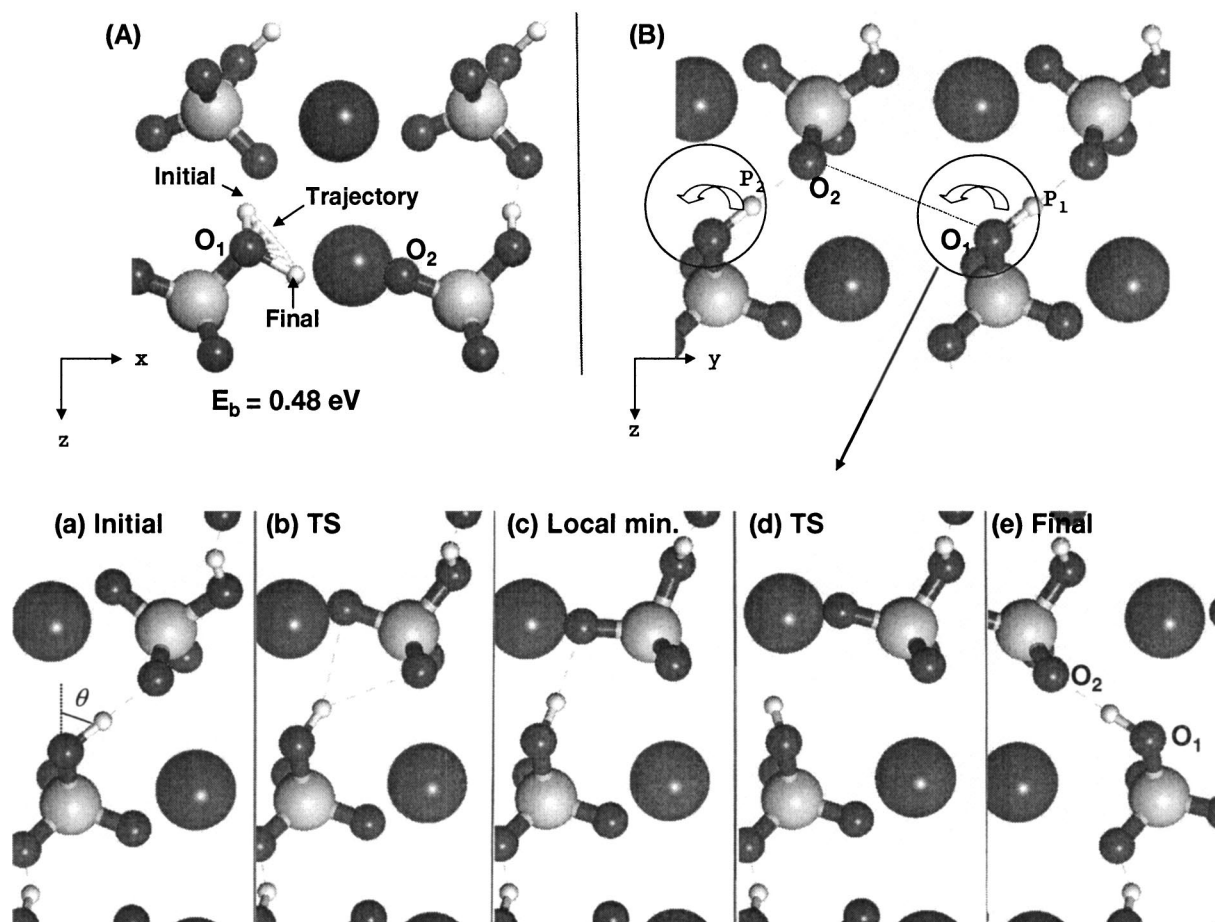


FIG. 9. Proton rotation around the oxygen ions in CHS-I. (A) and (B) represent the processes in the xz and yz planes, respectively. The process for (A) is illustrated as the trajectory, and the barrier for this process is 0.48 eV. The process for (B) is illustrated as the “snapshots,” in which *a* is initial state, *b* is TS, *c* is local minimum, *d* is another TS, and *e* is final state. The corresponding energy profile for the snapshots is shown in Fig. 10.

between O₁ and O₃. It can be seen from the figure that proton can be transferred from one hydrogen bond to the next by rotating with a barrier of 0.52 eV. Alternatively, from there proton may continue to transfer to the next oxygen ion. The barrier for proton transfer from O₁ to O₄ [in Fig. 8(a)] is 0.23 eV (not plotted). According to the above investigation, we can see that proton actually can transfer between the two oxygen ions within the tetrahedron indirectly, e.g., proton can transfer from O₂ to O₁ with a barrier of 0.25 eV [see Fig. 8(a) for the oxygen symbols], and then from there it can transfer to O₄ with a barrier of 0.23 eV.

4. Proton transfer to the next oxygen ion of the next-nearest-neighbor tetrahedron

Another possibility for a long-range proton diffusion can be made via a proton transfer to the NNN tetrahedron. For this process, we found that proton first rotates to a local minimum in order to make the distance between the two oxygen ions shorter (O-H bond is not broken), and then from there it continues to diffuse to the NNN tetrahedron. To address the problem explicitly, we divide the process into two parts: (a) Proton rotation around the oxygen ion, and (b) proton diffusion to the next oxygen ion of the NNN tetrahedron.

a. Proton rotation around the oxygen ion. For CHS-I, Figs. 9(A) and 9(B) illustrate proton rotation in the xz and yz planes, respectively. Figure 9(A) shows the trajectory of the rotation. In the final state, proton is located between O₁ and O₂. The barrier for this process is 0.48 eV. For a single proton rotation in the yz plane [in Fig. 9(B)], we found that there is no local minimum between O₁ and O₂. Therefore proton will come back once it is forced to rotate to the site between O₁ and O₂. Instead of this, we turn to investigate the concerted rotation, i.e., two protons rotate simultaneously. In this way there is a local minimum for the proton between O₁ and O₂. This may take place in the real diffusion, e.g., proton P₂ may rotate or diffuse to the other site, and then there is a local minimum for proton P₁ between O₁ and O₂. This rotation process is illustrated as the snapshots in Fig. 9, and the energy profile for this process is shown in Fig. 10, in which the symbols *a*, *b*, *c*, *d*, and *e* represent the initial-state, TS, local minimum, another TS, and final-state configurations, respectively. The barrier for this process is 0.24 eV.

Due to the highly ordered hydrogen-bond network in CHS-II, the hydrogen bonds are identical crystallographically. Therefore there is only one type of rotation in CHS-II.

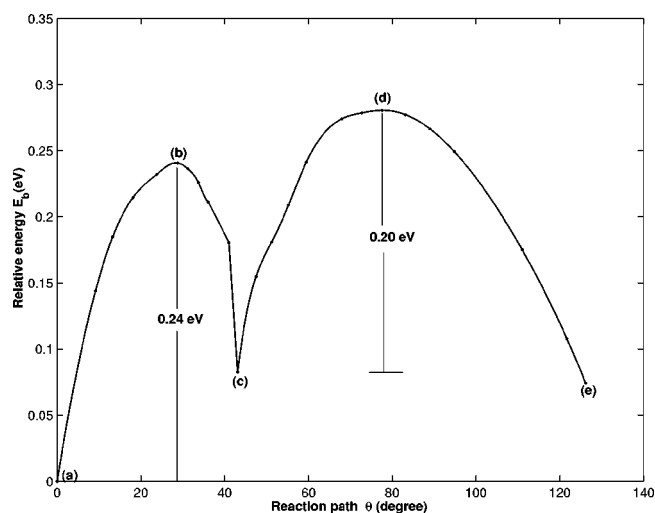


FIG. 10. The energy profile for the process of proton rotation in the yz plane [in Fig. 9(B)]. The symbols a , b , c , d , and e correspond to the “snapshots” in Fig. 9, in which a is initial state, b is TS, c is local minimum, d is another TS, and e is final state. The reaction path θ is defined in the snapshot a .

The process is illustrated in Fig. 11(A), and the energy profile for this process is presented in Fig. 11(B). Overall, the energy profile in this process is quite similar to that of CHS-I in Fig. 9(A) (that was not plotted).

b. Proton diffusion to the next oxygen ion of the NNN tetrahedron. After proton rotates to a local minimum, from there it may continue to diffuse to the NNN tetrahedron. The diffusion processes for CHS-I and CHS-II are illustrated in Fig. 12 and Fig. 13, respectively.

For CHS-I, Figs. 12(A) and 12(B) illustrate proton transfers in the xz and yz planes, respectively. The trajectory for proton transfer in the xz plane is illustrated in Fig. 12(A), and the energy profile for this process is shown in Fig. 12(C). The barrier for this process is 0.31 eV. Figure 12(B) actually shows proton transfer within the hydrogen bond. Therefore the barrier is quite low (0.20 eV).

According to the above investigation (in a and b) for CHS-I, the barriers for the proton rotation and diffusion in the yz plane are 0.24 eV and 0.20 eV, respectively, which are lower than those (0.48 eV and 0.31 eV) in the xz plane. But it should be noticed that there are two assumptions for the process in the yz plane, i.e., one is the concerted rotation, another is the concerted transfer within the hydrogen bond. Therefore, two processes (in the xz and yz planes) may coexist in the real proton diffusion.

For CHS-II, the trajectory for proton diffusion to the NNN tetrahedron is illustrated in Fig. 13(A), and the energy profile for the process is shown in Fig. 13(B). It can be seen from the figure that the barrier for this process is 0.87 eV, which is significantly higher than that of the similar process in CHS-I [0.31 eV in Fig. 12(C)]. In the final state, proton is located between O_2 and O_3 , rather than between O_1 and O_2 (because there is no local minimum between O_1 and O_2 in CHS-II). These are different from those in CHS-I. To get a better understanding of the differences, we have investigated

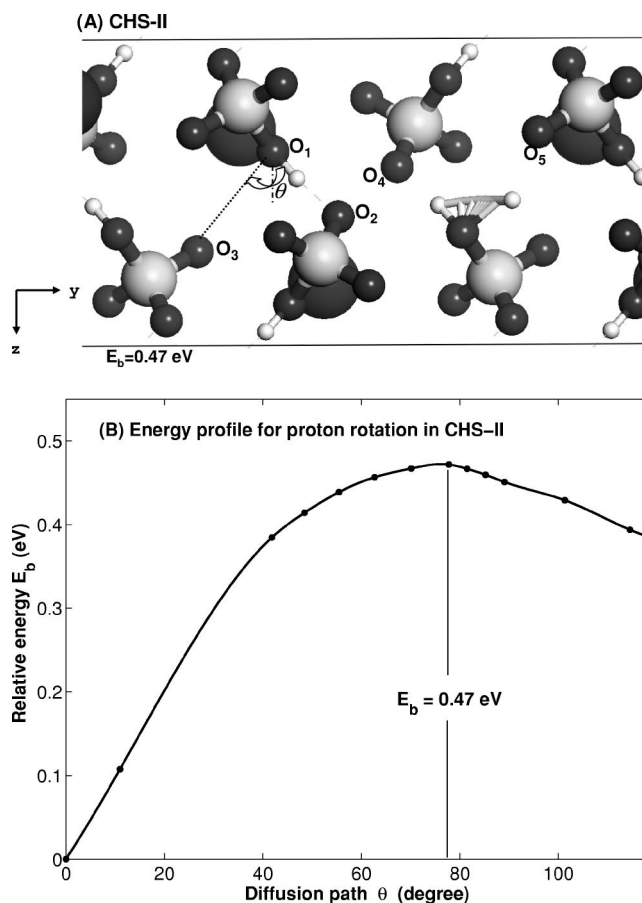


FIG. 11. Proton rotation around the oxygen ion in CHS-II. The process is illustrated as the trajectory in (A), and energy profile for this process is shown in (B). Note that some cesium ions are omitted for clarity.

the electron localization function (ELF) in the TS for CHS-I and CHS-II. The ELF is proved to be a useful tool to for studying bonded interactions^{32,33} since its definition by Becke *et al.*³⁴ The value of the ELF is between 0 and 1, and it will become relatively large in the regions with covalent bonds or lone pairs or unpaired electrons.^{32–34} Thus the covalent bonds or unpaired electrons can be classified based on the topological analysis of the ELF. We chose the ELF value in such a way that only the chemically relevant valence electrons (unpaired electrons) can be analyzed. The results are displayed in Fig. 14. It can be seen from the figure that the solid black domain (unpaired electrons) for proton in CHS-II is clearly distinguished, whereas this is not the case for CHS-I (see the arrows). It seems that the unpaired electrons should be responsible for the differences. In order to see the geometric change between the initial state and the TS, we specify $\Delta\theta$ by choosing the largest angle change in each structure in Fig. 14. It shows that $\Delta\theta$ ($=6.82^\circ$) in CHS-II is larger (almost double) than that (3.56°) in CHS-I. This means that the distortion of the tetrahedron in CHS-II is greater than that in CHS-I. This strain difference may be also related to these differences.

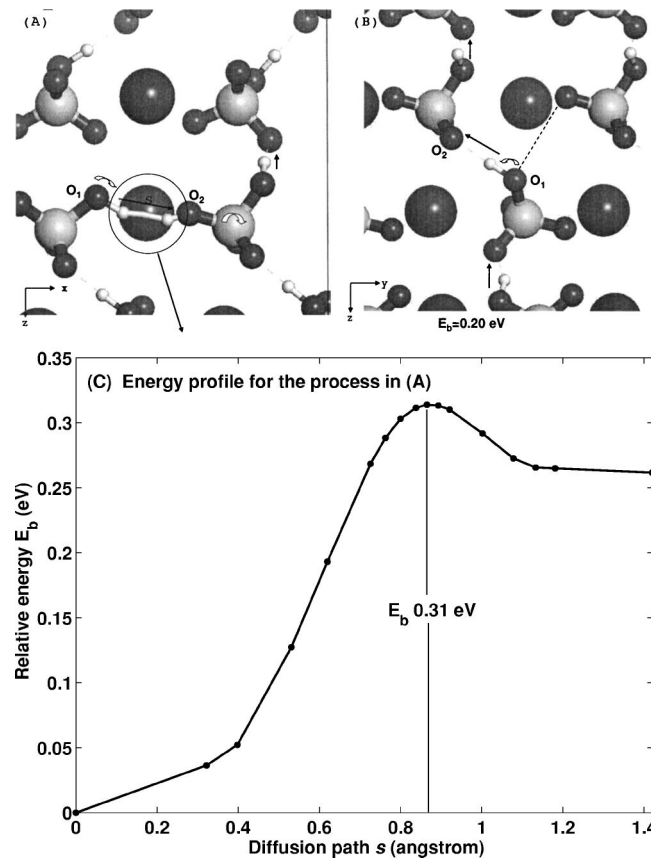


FIG. 12. After rotating, proton continues to diffuse to the next oxygen ion of the next-nearest-neighbor tetrahedron in CHS-I. (A) and (B) represent the processes in xz and yz planes, respectively. The energy profile for the process in (A) is shown in (C). The process in (B) is similar to that of proton transfer within the hydrogen bond.

Due to the light mass, proton quantum-mechanical tunneling may play an important role in these materials. This effect is neglected in our study. Kreuer considered that the proton tunneling in CHS-I is generally not important based on the analysis of the experimental data.¹⁴ This effect can be roughly discussed based on the proton-transfer processes and potentials. For proton transfer to the NN tetrahedron, it includes two processes. The first process is that the tetrahedron rotates, and then proton reaches a local minimum. The second process is that from that minimum proton continues to diffuse to the NN tetrahedron in the case of the concerted motion [see from *a* to *e* in Fig. 6(B)]. The first process means that there will be no local minimum (for proton) without the rotation of the tetrahedron, indicating that the dynamics of the tetrahedron is important. The second process means that proton can continue to diffuse only without a proton in the NN tetrahedron (or this proton is diffusing to other place). In other words, proton cannot continue to diffuse (including the tunneling) if the NN tetrahedron is HSO_4 formula (rather than SO_4). For proton transfer to the NNN tetrahedron, the situation is similar. From these analyses it indicates that the dynamics of the tetrahedrons is more important than the tunneling effect.

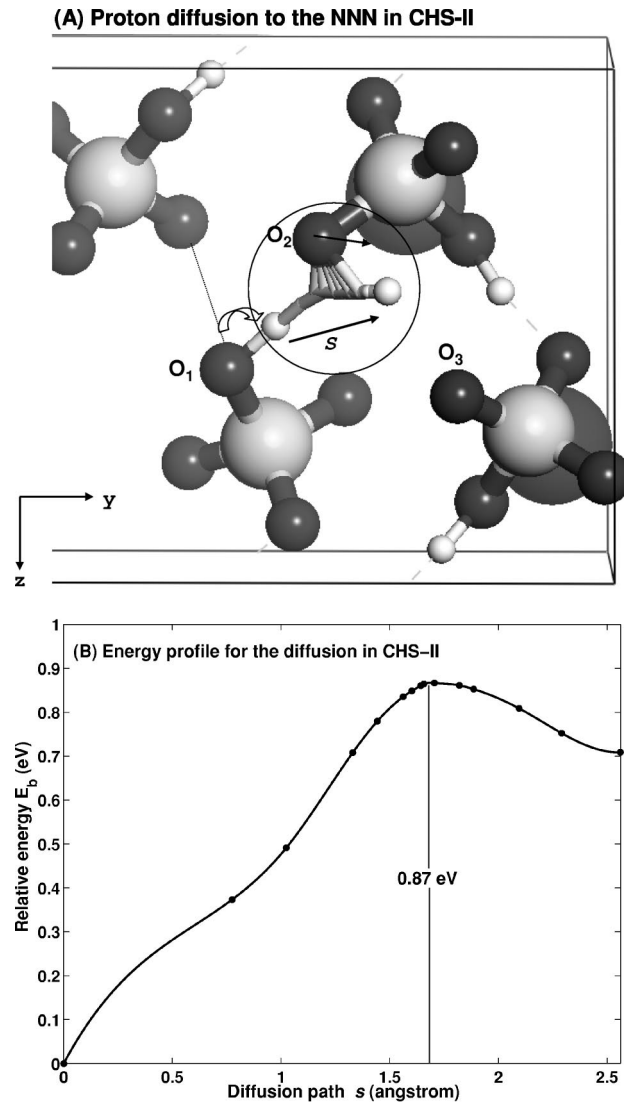


FIG. 13. After rotating, proton continues to diffuse to the next oxygen ion of the next-nearest-neighbor tetrahedron in CHS-II. The process is illustrated as the trajectory in (A). The energy profile for this process is shown in (B). The barrier is 0.87 eV, which is much higher than that (0.31 eV) of the similar process in CHS-I. The reaction path is roughly described by *s*.

IV. CONCLUSIONS

The electronic structure and the proton-transfer processes in phase I (CHS-I) and phase II (CHS-II) have been studied by density-functional calculations.

CHS-I and CHS-II have the same chemical formula with the different space group. CHS-I belongs to $I4_1/amd$ and CHS-II belongs to $P2_1/c$. The calculated results show that both phases have the similar DOS (or local DOS), and have almost the same band gap.

For proton transfer, we have systematically investigated the possible proton-transfer paths in two phases. The comparisons of the barriers between CHS-I and CHS-II are compiled in Table IV. The similarities are summarized as follows:

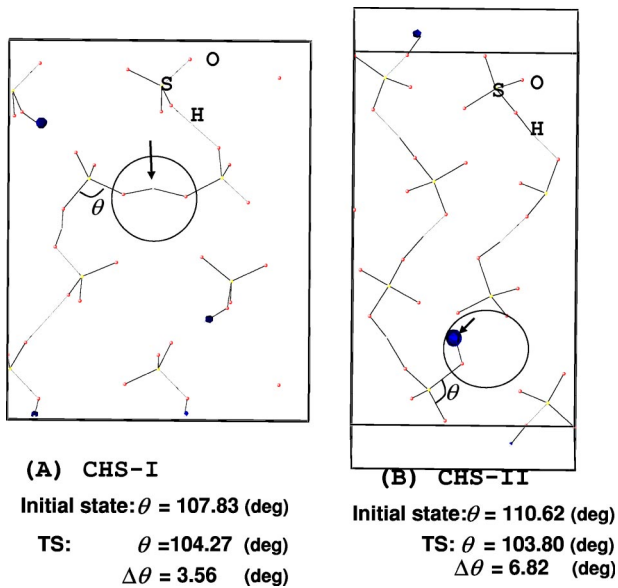


FIG. 14. The electron localization function (ELF) for the transition states (TS's) in the process of proton transfer to the next-nearest-neighboring (NNN) tetrahedron. (A) and (B) represent CHS-I and CHS-II, respectively. We chose ELF ($=0.88$) values in such a way that only the chemically relevant valence electrons (unpaired electrons) can be included. Note that all the cesium ions are omitted for clarity. The change of the largest distortion angle (degree) between the initial state and the TS is shown below the figure.

(a) Proton transfer within the sulfate tetrahedron is almost forbidden.

(b) Proton can jump forward and backward within the hydrogen bond.

The differences are summarized as follows.

(i) For proton transfer to the NN tetrahedron, this process is feasible for CHS-I, whereas it is almost forbidden for CHS-II.

(ii) Proton can transfer between the two oxygen ions within the tetrahedron indirectly in CHS-I, however this process is impossible for CHS-II (as discussed in the section of

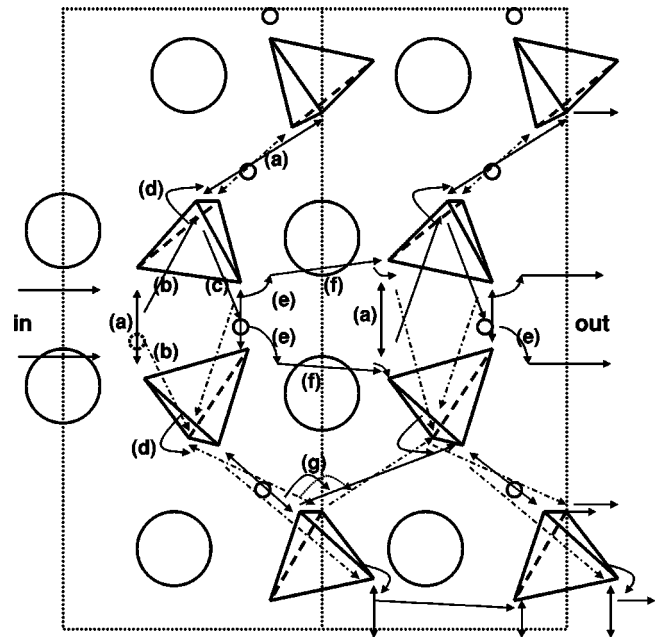


FIG. 15. The proposed proton-transfer mechanism in CHS-I. The symbols $a, b, d, e, f,$ and g represent the different processes. The arrow a represents the process that proton jumps forward and backward within the hydrogen bond. The arrows b and c represent the process that proton transfer to the nearest-neighboring (NN) tetrahedron, in which this process indicates that proton can transfer within the tetrahedron indirectly (as discussed in the section of proton transfer to the NN tetrahedron). d is the curved arrow, which represents the process that proton rotates from one hydrogen bond to the next (also see Fig. 8). The arrows e and f represent the processes that proton rotates to a local minimum, and then from there it continues to diffuse to the nearest-neighboring (NNN) tetrahedron. The arrow g represents the process that proton rotates from one hydrogen bond to the next [also see Fig. 9(B)].

proton transfer to the NN tetrahedron).

(iii) For proton transfer to the NNN tetrahedron, there are two types of the proton-transfer paths in CHS-I, whereas there is only one type in CHS-II. The diffusion barrier in

TABLE IV. The comparisons of the diffusion barriers between CHS-I and CHS-II in the following processes: (1) proton transfer within the tetrahedron, (2) proton transfer within the hydrogen bond, (3) proton transfer to the nearest-neighboring (NN) tetrahedron, and (4) proton transfer to the next-nearest-neighboring (NNN) tetrahedron. The item (4) contains (a) proton rotation and (b) proton diffusion. For CHS-I, there are two types of proton rotation and diffusion to the NNN tetrahedron. The similarity and difference are denoted as \checkmark and \times , respectively. The measured barriers for CHS-I are 0.3–0.4 eV (Ref. 3). Units are in eV.

Processes	CHS-I	CHS-II	Similar process?	Remarks
(1) Transfer within tetrahedron	1.54	1.73	\checkmark	Almost forbidden
(2) Transfer within hydrogen bond	0.16	0.17	\checkmark	Feasible
(3) Transfer to NN tetrahedron	0.25, 0.11	No	\times	Forbidden for CHS-II
(4) Transfer to NNN tetrahedron				
(a) Proton rotation				
Type 1	0.48	0.47	\checkmark	
Type 2	0.24, 0.20	No	\times	
(b) Proton diffusion				
Type 1	0.31	0.87	\times	A large barrier for CHS-II
Type 2	0.20	No	\times	

CHS-II is much higher than that in CHS-I.

For proton transfer to the NN tetrahedron, the arrangement of the hydrogen-bond network should be responsible for the difference between the two phases. Due to the highly ordered hydrogen-bond network in CHS-II, it makes the re-orientation of the tetrahedron very difficult. The relatively disordered hydrogen-bond network in CHS-I makes the re-orientation easy, and consequently proton can be easily transferred to the NN tetrahedron.

Based on the above analyses, the proton-transfer mechanism in CHS-I is proposed in Fig. 15. The symbols *a*, *b*, *d*, *e*, *f*, and *g* represent the different proton-transfer processes. The arrow *a* represents the process that proton jumps forward and backward within the hydrogen bond. The arrows *b* and *c* represent the processes that proton transfers to the NN tetrahedron, in which this process also indicates that proton can transfer between the two oxygen ions within the tetrahedron indirectly. *d* is the curved arrow, which represents the process that proton rotates from one hydrogen bond to the next (also see Fig. 8). The arrows *e* and *f* represent the processes that proton rotates to a local minimum, and then from there it continues to diffuse to the NNN tetrahedron. The curved arrow *g* represents the process that proton rotates from one hydrogen bond to the next. Overall, the diffusion picture looks like that proton jumps forward and backward within the hydrogen bond (arrow *a*), sometimes

proton transfers to the NN tetrahedron (arrow *b*), and from there it continues to transfer to the next oxygen ion (arrow *c*) or to the next hydrogen bond (arrow *d*), sometimes proton rotates to a local minimum, and from there it continues to transfer to the NNN tetrahedron (arrows *e* and *f*).

The current study indicates that there are multiple proton-transfer processes in CHS-I. The calculated results show that proton cannot transfer between the two oxygen ions within the tetrahedron directly. This is somewhat different from the proposal by Belushkin *et al.*, who drawn a straight line between the two points.^{26,35} In addition, the processes including proton transfer to the NN tetrahedron and proton rotation from one hydrogen bond to the next were lacking in their proposal. We expect that the established model also is valid for the superionic family (with the same structure) such as CsHSeO₄ and RbHSeO₄.

ACKNOWLEDGMENTS

The authors thank Dr. T. Yamamoto and Dr. K. Tatsumi for useful technical help, and Dr. L. N. Kantorovich³⁶ and Dr. Jay Sullivan for their nice scripts, and financial support of MEXT Japan on Computational Materials Science Unit in Kyoto University.

*Electronic address: ke@fukui.kyoto-u.ac.jp, xzke@yahoo.com

†Electronic address: Tanaka@cms.mtl.kyoto-u.ac.jp

¹J. H. Hirschenhofer, D. B. Stauffer, R. R. Engleman, *Fuel Cell Technology Handbook* (CRC Press, Boca Raton, 2003).

²H. Iwahara, *Solid State Ionics* **86-88**, 9 (1996).

³A.I. Baranov, L.A. Shuvalov, and N.M. Shchagina, *JETP Lett.* **36**, 459 (1982).

⁴S.M. Haile, D.A. Boysen, C.R.I. Chisholm, and R.B. Merle, *Nature (London)* **410**, 910 (2001).

⁵A.V. Belushkin, I. Natkaniec, N.M. Pakida, L.A. Shuvalov, and J. Wasicki, *J. Phys. C* **20**, 671 (1987).

⁶A.M. Balagurov, A.V. Belushkin, I.D. Dutt, I. Natkaniec, M. Pakida, B.N. Savenko, L.A. Shuvalov, and J. Wasicki, *Ferroelectrics* **63**, 59 (1985).

⁷Superprotonic Phase Transitions in Solid Acids: Parameters affecting the presence and stability of superprotonic transitions in the MH_nXO₄ family of compounds (X=S, Se, P, As; M=Li, Na, K, NH₄, Rb, Cs), C. R. I. Chisholm (Ph.D. thesis, California Institute of Technology, Pasadena, California, 2003).

⁸A.I. Baranov, B.V. Merinov, A.V. Tregubchenko, V.P. Khiznichenko, L.A. Shuvalov, and N.M. Schagina, *Solid State Ionics* **36**, 279 (1989).

⁹V.V. Sinityn, E.G. Ponyatovski, A.I. Baranov, A.V. Tregubchenko, and L.A. Shuvalov, *Sov. Phys. JETP* **73**, 386 (1991).

¹⁰R. Blinc, J. Dolinsek, G. Lahajnar, I. Zupancic, L.A. Shuvalov, and A.I. Baranov, *Phys. Status Solidi B* **123**, K83 (1989).

¹¹W. Münch, K.D. Kreuer, U. Traub, and J. Maier, *Solid State Ionics* **77**, 10 (1995).

¹²W. Münch, K.D. Kreuer, U. Traub, and J. Maier, *J. Mol. Struct.* **381**, 1 (1996).

¹³C.R.I. Chisholm and S.M. Haile, *Mater. Res. Bull.* **35**, 999 (2000).

¹⁴K.D. Kreuer, *Chem. Mater.* **8**, 610 (1996).

¹⁵J.C. Badot and Ph. Colomban, *Solid State Ionics* **35**, 143 (1989).

¹⁶G. Kresse and J. Furthmüller, *Comput. Mater. Sci.* **6**, 15 (1996).

¹⁷G. Kresse and J. Furthmüller, *Phys. Rev. B* **54**, 11 169 (1996).

¹⁸J.P. Perdew, J.A. Chevary, S.H. Vosko, K.A. Jackson, M.R. Pederson, D.J. Singh, and C. Fiolhais, *Phys. Rev. B* **46**, 6671 (1992).

¹⁹P.E. Blöchl, *Phys. Rev. B* **50**, 17 953 (1994).

²⁰G. Kresse and D. Joubert, *Phys. Rev. B* **59**, 1758 (1999).

²¹H.J. Monkhorst and J.D. Pack, *Phys. Rev. B* **13**, 5188 (1976).

²²H. Jónsson, G. Mills, and K. M. Jacobsen, in *Nudged Elastic Band Method for Finding Minimum Energy Paths of Transitions in Classical and Quantum Dynamics in Condensed Phase Simulations*, edited by B. J. Berne, G. Ciccotti, and D. F. Coker (World Scientific, Singapore, 1998).

²³Z. Jirak, M. Dlouha, S. Vratilav, A.M. Balagurov, A.I. Beskrovnyi, V.I. Gordelii, I.D. Datt, and L.A. Shuvalov, *Phys. Status Solidi A* **100**, K117 (1987).

²⁴B.V. Merinov, A.I. Baranov, L.A. Shuvalov, and B.A. Maksimov, *Kristallografiya* **32**, 86 (1987).

²⁵A.V. Belushkin, W.I.F. David, R.M. Ibberson, and L.A. Shuvalov, *Acta Cryst.* **47**, 161 (1991).

²⁶A.V. Belushkin, C.J. Carlile, W.I.F. David, R.M. Ibberson, L.A. Shuvalov, and W. Zajac, *Physica* **174**, 268 (1991).

²⁷Ground-state structure of CsHSO₄ in phase I (unpublished).

²⁸S.T. Pantelides, D.J. Mickish, A.B. Kunz, *Phys. Rev. B* **10**, 5203 (1974).

²⁹R.O. Jones and O. Gunnarsson, *Rev. Mod. Phys.* **61**, 689 (1989).

³⁰E. Fois and A. Gamba, *J. Phys. Chem. B* **103**, 1794 (1999).

- ³¹M.S. Islam, R.A. Daveis, and J.D. Gale, *Chem. Commun. (Cambridge)* **7**, 661 (2001).
- ³²A. Savin, R. Nesper, S. Wengert, and T.F. Fassler, *Angew. Chem., Int. Ed. Engl.* **36**, 1808 (1997).
- ³³B. Silvi and A. Savin, *Nature (London)* **371**, 683 (1994).
- ³⁴A.D. Becke and K.E. Edgecombe, *J. Chem. Phys.* **92**, 5397 (1990).
- ³⁵A.V. Belushkin, M.A. Adams, S. Hull, and L.A. Shuvalov, *Solid State Ionics* **77**, 91 (1995).
- ³⁶L.N. Kantorovich, user-friendly visualization program for plane-wave DFT codes, 1996-2002 (see <http://www.cmmmp.ucl.ac.uk/~lev/codes/lev00/>).